



Article

Research on the Classification of Concrete Sulfate Erosion Types in Tumushuke Area, Xinjiang

Yuwei Ma ¹ , Xuemei Jiang ¹, Junfeng Li ^{1,*} , Gang Li ^{1,*}, Wei Huang ², Weidong Chang ¹, Guangming Cao ² and Ziwei Yu ¹

¹ College of Water Conservancy & Architectural Engineering, Shihezi University, Shihezi 832000, China; myw819@shzu.edu.cn (Y.M.); jxm123ii@sina.com (X.J.); wdchang@stu.shzu.edu.cn (W.C.); yzwww1028@sina.com (Z.Y.)

² Xinjiang Qiankun Engineering Construction Group, Tumushuke City 843900, China; huangwei17173@sina.com (W.H.); xjshzcgms@sina.com (G.C.)

* Correspondence: lijunfeng@shzu.edu.cn (J.L.); gangli@shzu.edu.cn (G.L.); Tel.: +86-152-9992-1362 (J.L.); +86-182-0905-2819 (G.L.)

Abstract: Tumushuke, a significant node of “the China–Pakistan Economic Corridor” and “the Silk Road Economic Belt”, is strategically located in the southern region of Xinjiang. Due to the widespread distribution of its salty soils, concrete construction safety is significantly compromised. The construction of this project used sulfate-resistant cement, which was costly to construct. Six groups with varying sulfate immersion concentrations were set up to perform sulfate erosion tests and sulfate freeze–thaw coupling tests, respectively, based on the survey of the distribution of sulfate concentration in the area. The Tumushuke area’s concrete erosion kinds were classified using a microanalysis of the degraded concrete. The findings indicate that the concrete primarily exhibits gypsum-type erosion when the sulfate concentration is greater than 20,000 mg/kg, ettringite–gypsum-type erosion when the sulfate concentration is between 15,000 and 20,000 mg/kg, and ettringite–gypsum-type erosion when the sulfate concentration is less than 15,000 mg/kg. The erosion product, carbon–sulfur silica–calcite, also occurs under sulfate freeze–thaw coupling. In the Tumushuke area, ettringite-type erosion damage is primarily found in low-sulfate areas in the southwest and a small portion of the northeast. In contrast, higher-sulfate areas in the central northward area are primarily affected by ettringite–gypsum and gypsum-type erosion damage. The results of this study can provide a basis for adopting different anti-sulfate erosion measures for engineering construction in different regions.

Keywords: Tumushuke area; concrete; sulfate erosion; types of erosion damage



Citation: Ma, Y.; Jiang, X.; Li, J.; Li, G.; Huang, W.; Chang, W.; Cao, G.; Yu, Z. Research on the Classification of Concrete Sulfate Erosion Types in Tumushuke Area, Xinjiang. *Buildings* **2024**, *14*, 729. <https://doi.org/10.3390/buildings14030729>

Academic Editor: Giuseppe Santarsiero

Received: 26 January 2024

Revised: 23 February 2024

Accepted: 4 March 2024

Published: 8 March 2024



Copyright: © 2024 by the authors. Licensee MDPI, Basel, Switzerland. This article is an open access article distributed under the terms and conditions of the Creative Commons Attribution (CC BY) license (<https://creativecommons.org/licenses/by/4.0/>).

1. Introduction

The most popular building material in engineering is concrete, but environmental conditions can quickly reduce its strength and lifespan. Xinjiang is located in the hinterland of the Eurasian continent, and the area of saline soil accounts for 22.01% of the total area of saline soil in China. It is the area of China where saline soils are most widely distributed, where there are the most varieties of salinization, and where soil salt buildup is the highest. Saline soils, because of their high SO_4^{2-} content, seriously affect the longevity and safety of concrete constructions [1,2] and seriously jeopardize the service life of concrete buildings in the area [3–5]. The Tumushuke area is situated in southern Xinjiang. It is a significant node in “the China–Pakistan Economic Corridor” and “the Silk Road Economic Belt”. The region has a diverse climate and a wide distribution of saline soil. The region is very strongly represented by the use of sulfate-resistant cement for engineering and construction, and the high cost of engineering and construction, which will be very representative of the study of sulfate erosion in southern Xinjiang. Therefore, the Tumushuke area was chosen as the study area. A survey of SO_4^{2-} and Cl^- in the area’s soils indicated that the soils were all

sulfite saline soils. Its soils were extremely saline in terms of SO_4^{2-} and Cl^- , and both peak concentrations occurred in the northeastern part of Tumushuke [6], and by investigating the distribution of sulfate throughout the region, different sulfate concentration gradients were taken to analyze the sulfate erosion products at different concentrations and to classify the type of sulfate erosion in different areas. Finally, different anti-erosion measures were taken for different erosion products. This will be important in reducing the cost of construction and guiding the construction of projects in the Tumushuke area.

The process of erosion damage caused by SO_4^{2-} in the soil on concrete is quite complicated; the two primary types of damage are chemical and physical erosion damage [7]. When the concrete goes from a wet to a dry condition, sulfate hydrate precipitates within the pores, causing physical erosion damage. Its crystal volume expands throughout the crystallization process, which breaks down the structure of the concrete by producing a tremendous pressure inside the pores known as the crystallization pressure [8]. As far as chemical erosion is concerned, one of the important factors is external sulfate erosion. A large body of research on sulfate attack on concrete has been conducted in the last few decades [9–11], with some findings indicating that gypsum ($\text{CaSO}_4 \cdot 2\text{H}_2\text{O}$) and ettringite ($3\text{CaO} \cdot \text{Al}_2\text{O}_3 \cdot 3\text{CaSO}_4 \cdot 32\text{H}_2\text{O}$) are the most often occurring products of sulfate attack [12,13]. In addition, carbon–sulfur silica–calcite-type erosion (TSA) occurs in addition to ettringite erosion and gypsum-type erosion [14]. The parameters for TSA are more complicated than those for ettringite and gypsum erosion; it needs temperatures below 15°C and the presence of CO_3^{2-} in the concrete aggregate [15]. However, TSA-type erosion damages the concrete structure by directly dissolving the C-S-H gel and lowering the internal bonding of the concrete rather than significantly expanding the concrete. Thus, in sulfate-rich environments, chemical erosion is thought to be the primary cause of concrete performance decline [16].

It has been shown that the sulfate concentration in the environment affects the type of erosion products [17]. Thus, to classify the type of erosion and investigate the types of erosion products under various sulfate concentrations, the sulfate concentration in saline soils in the Tumushuke area can be graded. This will create a database for the prevention and control of concrete sulfate erosion damage in the future. The Tumushuke area is a seasonal permafrost region, and freeze–thaw cycles and sulfate erosion both harm concrete in this area. The predominant type of cement used in local engineering construction is anti-sulfate cement, which has a cost per m^3 of concrete that is approximately 100¥ more than that of regular silicate concrete. Consequently, thorough the investigation and examination of concrete materials in the context of sulfate erosion and the freeze–thaw cycle under the coupling effect of the erosion type is particularly important for taking various anti-sulfate erosion measures during the project’s subsequent construction to lower project costs while also having a significant practical meaning.

2. Test Method

2.1. Design of Test Scheme

A prior study [6] found that the Tumushuke area’s saline soils were primarily sulfite saline soils, with 29,380 mg/kg of SO_4^{2-} being the highest concentration in this area. The trend of “high in the east and low in the west” and “high in the north and low in the south” was generally evident in the horizontal distribution of soil salinity, with the northeastern region of Tumushuke exhibiting the highest concentration. Its specific distribution is shown in Figure 1.

The concrete structures in the Tumushuke area of Xinjiang, which is part of the seasonal permafrost region and experiences a high degree of day-to-night temperature differential due to its perpetual drought and low rainfall, are vulnerable to both soil erosion from SO_4^{2-} and freezing–thawing damage. Consequently, six groups of sulfate leaching solutions were made up of varying concentrations of 0 mg/kg, 5000 mg/kg, 10,000 mg/kg, 15,000 mg/kg, 20,000 mg/kg, and 30,000 mg/kg based on the study and measurement of SO_4^{2-} concentration in saline soils in the Tumushuke area. Upon reaching the designated

curing age, the specimens were split into six groups and submerged in the six concentrations of prepared solutions, with the specimens positioned at least 20 mm below the liquid's surface. Every 30 days, the soaking solution was changed, and every 7 days, the soaking solution's pH was determined. The specimens were cured for 28 days in a standard curing box. After being removed from the curing box, the specimens were submerged in water for 4 days. Following this, the water on the specimens' surface was wiped off, and the pertinent data were measured. Using the "fast freezing method" described in GB-T50082-2009 [18], every twenty-five freeze–thaw cycles, the test blocks were taken out, any water that had formed on the surface was wiped away with a towel, and the test blocks' mass, dynamic elastic modulus, and compressive strength were measured. After that, it was installed once again for freeze–thaw cycles to complete the sulfate freeze–thaw coupling test and the entire immersion test of concrete. Owing to the Tumushuke area's 138 mg/L groundwater sulfate concentration and the high concentration of SO_4^{2-} in the soil, the total concentration of the soaking solution equaled the total concentration of sulfate in the groundwater before and after sulfate was added when using groundwater to soak the concrete. After 28 days of curing, the constructed concrete specimens were submerged in various sodium sulfate solution concentrations for 270 days. XRD, SEM, and IR (The D/max-2550 X-ray diffraction (XRD) with the angular range of $5\text{--}60^\circ$ and a minimum scanning step size of 0.01° was provided by Rigaku Corporation in Tokyo Metropolis Akishima-shi, Japan. The SU8000 cold field emission scanning electron microscope from Hitachi, Chiyoda-ku, Tokyo, Japan, was used to measure microstructure. The VERTEX 70v Fourier-transform infrared spectroscopy (FTIR) made by Bruker Corporation in Billerica, MA, USA, with a wave number range of $400\text{--}4000\text{ cm}^{-1}$ and a distinguishability of 1 cm^{-1} was used to determine the functional group of hydrations.) The analyses of the erosion products were then used to identify the kind of sulfate erosion that had occurred in the Tumushuke area.

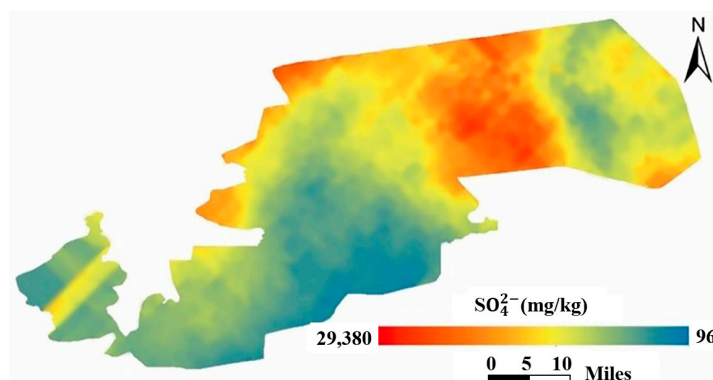


Figure 1. SO_4^{2-} distribution of surface soil in the Tumushuke area [6].

To conduct the sulfate erosion test, the specimens that have reached the required curing age are divided into six groups and submerged in the six concentrations of prepared solutions, with the specimens submerged at least 20 mm below the liquid's surface. The soaking solution was changed every 30 days and removed for testing. In the Tumushuke area, the freeze–thaw minimum temperature of -25°C was selected due to the extremely low temperature of -24.2°C . To perform the sulfate freeze–thaw coupling test, we used the "fast freezing method" described in GB-T50082-2009 [18].

2.2. Test Raw Materials

The test used P·O42.5 ordinary silicate cement, and Table 1 displays the pertinent indices. The coarse aggregate was chosen from continuous graded gravel with lengths of 5–20 mm and 20–40 mm; the corresponding indices are shown in Tables 2 and 3. Tables 4 and 5 display the pertinent indices for the fine aggregate, which was chosen to be coarse sand with a fineness modulus of 3.4. Anhydrous sodium sulfate served as the erosion solution solute, while high-performance polycarboxylic acid was used as

the water reduction agent, and regular tap water served as the test water. According to GB/T50081-2019 “Standard for test method of mechanical and physical performance on concrete” [19], the size of coarse aggregate was less than 40 mm, the test molding size was 100 mm × 100 mm × 100 mm, and the concrete mark was selected as C30. Table 6 displays the quantity of concrete materials utilized.

Table 1. Fundamental chemical and physical characteristics of cement technical indicators.

Item	Standard Consistence/%	Initial Setting Time/min	Final Setting Time/min	Compressive Strength/MPa		Break off Strength /MPa	
				3 d	28 d	3 d	28 d
Technology Index	27.4	≥45	≤600	≥17.0	≥42.5	≥3.5	≥6.5
P·O42.5	27.4	181	227	29.4	46.5	6.0	8.9

Table 2. Coarse aggregate indicators.

Item	Soil Content/%	Mud Content /%	Crush Value /%	Apparent Density /(kg/m ³)
Quality Index	≤1.0	≤0.5	≤12	≥2600
5–20 mm Gravel	0.6	0.3	9.5	2720
20–40 mm Gravel	0.6	0.4	—	2740

Table 3. Coarse aggregate particle gradation.

Nominal Particle Size/mm	80.0	63.0	50.0	40.0	31.5	25.0	20.0	16.0	10.0	5.00	2.50
Standard Particle Grading Range Cumulative Sieve Residue/%	/	/	/	0~10	/	/	80~100	/	95~100	/	/
Actual Cumulative Sieve Residue/%	/	/	/	2	39	64	83	91	98	100	100

Table 4. Fine aggregate performance indicators.

Item	Soil Content	Mud Content /%	Apparent Density/(kg/m ³)	Volume Density/(kg/m ³)
Technology Index	≤3.0	≤1.0	≥2500	≥1400
Fine Aggregate	2.9	0.7	2720	1690

Table 5. Fine aggregate particle gradation.

Nominal Particle Size		10.0 mm	5.0 mm	2.50 mm	1.25 mm	630 μm	315 μm	160 μm
The Standard Requires	I	0	10~0	35~5	65~35	85~71	95~80	100~90
Cumulative Sieve Residue/%	II	0	10~0	25~0	50~10	70~41	92~70	100~90
Actual Cumulative Sieve Residue/%	III	0	10~0	15~0	25~0	40~16	85~55	100~90
Actual Cumulative Sieve Residue/%		0	5	31	51	72	87	100

Table 6. Proportioning of concrete.

Supplies	Crushed Coarse Aggregate /(kg/m ³)	Fine Aggregate /(kg/m ³)	Cement /(kg/m ³)	Water /(kg/m ³)	Admixture /(kg/m ³)
Dosage	1000	840	425	180	5

3. Analysis and Discussion of Results

3.1. Concrete Strength

3.1.1. Full Immersion Test of Concrete

Figure 2 displays the results of testing on the fully immersed concrete's compressive strength. With increasing erosion age, the concrete specimens' compressive strengths first showed an increasing tendency before declining. During the initial phase of erosion, the hydration of the concrete specimen was enhanced by the reaction between sulfate and cement hydration, which generated some ettringite to fill the pores of the concrete specimen. The expanding internal stress that results did not cause the concrete specimen to crack because it had not yet reached the concrete's tensile strength. Rather, ettringite crystals were packed into the interior pores of the concrete specimens, increasing their density and strengthening the porous skeletal structure. Thus, early in the immersion process, there was an increase in compressive strength. However, as the erosion age increased, the hydration reaction inside the specimen continued unabatedly, producing an increasing number of erosion products inside the concrete specimen. As a result, the internal stress within the concrete expanded quickly until it surpassed its tensile strength, causing the specimen to develop microcracks that caused the compressive strength to decrease once more as the erosion age increased. Simultaneously, the specimen's internal microcracks facilitated the infiltration of external sulfate ions into the concrete. This cycle was repeated, eventually leading to a macrostructure deformation of the concrete and producing macroscopic large cracks, spalling, and other surface phenomena. This resulted in a decrease in the specimen's macro-mechanical deformation properties, a reduction in its toughness, an increase in its rigidity, and a shift in the damage pattern from dilative shear failure to brittle failure.

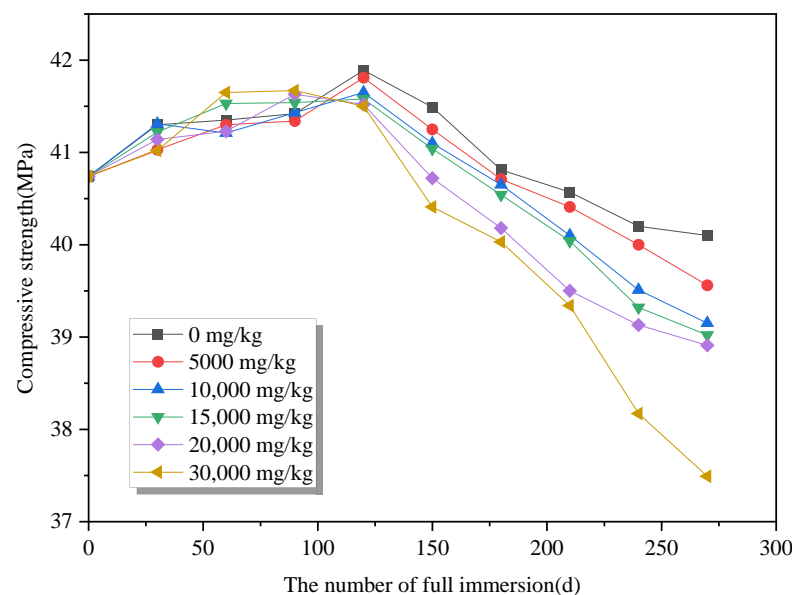


Figure 2. Curve of compressive strength with the age of erosion at different sulfate concentrations.

In comparison to immersion for 0 d, the specimens' compressive strength decreased by 1.57%, 2.90%, 3.90%, 4.22%, 4.49%, and 7.98% at the erosion age of 270 d. That is, after about 120 d, the higher the sulfate concentration, the smaller the compressive strength values of the eroded concrete specimens, and the higher the sulfate concentration, the longer the age of erosion, and the faster the rate of compressive strength decrease.

3.1.2. Concrete Sulfate Freeze–Thaw Coupling Tests

As illustrated in Figure 3, specimens of concrete exhibit a slight gain in compressive strength at 25 freezing and thawing cycles, which is followed by a drop in the specimen's compressive strength as the number of cycles increases. The increase in compressive

strength at 25 freeze–thaw cycles is due to the reaction of sulfate with cement hydration to form the hydration products ettringite and gypsum, which in turn fill the pores within the concrete and are not sufficient to cause expansion cracks in the specimens. On the other hand, a higher densification of the specimen will lead to a higher compressive strength. At 225 cycles of freeze–thaw, the specimens' compressive strengths are 74.19%, 71.89%, 69.34%, 68.38%, 66.09%, and 64.93% of their original strengths, in that order. It is evident that the specimen's compressive strength value steadily drops as the sulfate solution concentration rises; in other words, the greater the sulfate solution concentration, the lower the specimen's compressive strength value during the freeze–thaw cycle test.

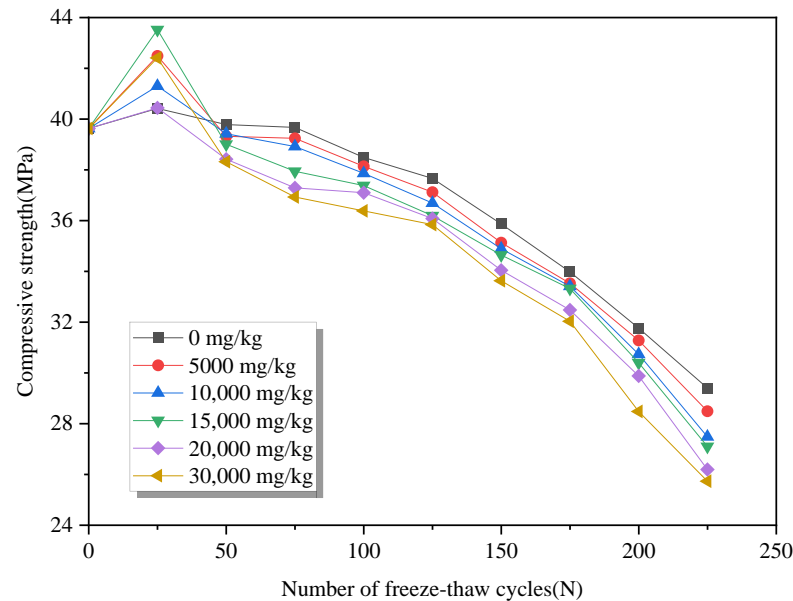


Figure 3. Variation curves of compressive strength of concrete specimens after coupling action of sulfate freeze–thaw cycles.

3.2. Analysis of X-ray Diffraction Results

3.2.1. Full Immersion Test of Concrete

The XRD test results are shown in Figure 4. It is evident that the concrete specimens that were cured with deionized water for 28 days contained SiO_2 , CaCO_3 , $\text{Ca}(\text{OH})_2$, and small ettringite diffraction peaks. Additionally, aggregates were the primary cause of the CaCO_3 and SiO_2 diffraction peaks, which were relatively high and stable. The $\text{Ca}(\text{OH})_2$ diffraction peaks, on the other hand, became weaker and the diffraction peaks of ettringite and gypsum manifestly strengthened after the specimens were submerged in the sulfate solution for 270 days. This was because of a chemical reaction that occurred between the sulfate that entered the concrete's interior and the cement's hydration products. In the process, the specimen's $\text{Ca}(\text{OH})_2$ was consumed, and erosion products like ettringite and gypsum were produced. These products showed up macroscopically as the specimen deteriorated and was destroyed [20,21]. Soaking in the sulfate-containing (138 mg/L) local groundwater produced ettringite diffraction peaks in concrete specimens with an SO_4^{2-} concentration of 0 mg/kg.

XRD reveals comparatively low-intensity diffraction peaks of gypsum and ettringite in concrete specimens at 270 days of specimen immersion under low concentrations of sulfate solution immersion, and the diffraction peaks of the erosion products are gradually enhanced with the increase in sulfate concentration. This is caused by the formation of ettringite (10–50 nm) in the concrete's tiny pores when the concentration of external sulfate rises. This creates a stress of approximately 8 MPa, which is greater than the substrate's tensile strength (3–4 MPa), and it also raises the cement's expansion pressure [22]. The intensity of the diffraction peaks of ettringite reduced marginally while the intensity of

the characteristic peaks of gypsum increases dramatically when the SO_4^{2-} concentration is greater than 15,000 mg/kg. The reason for this is that the specimen's $\text{Ca}(\text{OH})_2$ is consumed by the sulfate solution in the pores due to the high sulfate environment. This lowers the pH of the pore solution inside the concrete, causes the C-S-H to break down unstably, and dissolves a significant amount of calcium ions [23–26]. These calcium ions react with SO_4^{2-} in the pores to form gypsum, thus leading to a significant increase in gypsum content. Studies by Ma X and Liu F. also demonstrated that pores with sizes ranging from 10 to 70 nm filled one after the other during immersion and that higher sulfate solutions caused the pores to fill more quickly [27,28]. The high sulfate solution causes increased sulfur content along the diffusion direction for the same immersion duration. Distributed cracks also continue to grow into continuous microcracks and continue to deposit gypsum in the cracks. As a result, concrete specimens show primarily gypsum-type erosion in situations with high sulfate content.

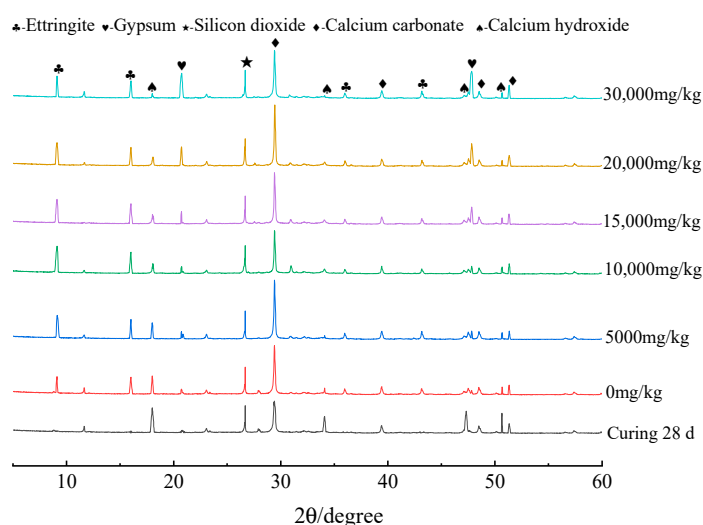


Figure 4. XRD plots for 28 days of conservation and 270 days of full immersion.

3.2.2. Concrete Sulfate Freeze–Thaw Coupling Tests

The concrete specimens were subjected to the sulfate freeze–thaw coupling test, and the results showed that the concrete's erosion products changed according to the same rule as in the full immersion test with 225 freeze–thaw cycles and varying sulfate immersion concentrations. Figure 5 illustrates how the intensity of the $\text{Ca}(\text{OH})_2$ diffraction peaks progressively reduced as the immersion period increased, while the ettringite and gypsum diffraction peaks were enhanced. This suggested that the $\text{Ca}(\text{OH})_2$ within the concrete specimens undergoes a chemical reaction with the sulfate within the pores during the freeze–thaw cycle, which consumes a significant amount of $\text{Ca}(\text{OH})_2$ and lowers its concentration. At the same time, erosion products such as ettringite and gypsum are also generated [29,30]. Furthermore, because of the concrete's very sluggish chemical attack, the diffraction peaks for gypsum had substantially lower intensities than the diffraction peaks in the full immersion test. Because SO_4^{2-} ions from the external sulfate environment enter the concrete specimen's interior, during freeze–thaw cycles, more slowly, the concentration of diffusible SO_4^{2-} ions in the specimen is low, making it challenging to form stable gypsum crystals in this environment [31,32]. Nevertheless, gypsum forms when the concrete specimen's diffusible SO_4^{2-} ion concentration rises due to the specimen's deteriorating structure.

Unlike the sulfate full immersion test, the sulfate freeze–thaw coupling condition exposes the concrete specimens to low temperatures for an extended period. In this scenario, the hydration products of the cement react with the Ca^{2+} , SO_4^{2-} , and CO_3^{2-} in the concrete specimens' pore fluid to produce carbon–sulfur calcium silica [33]. Figure 5 also shows a double-headed peak at 9° and 16° , as well as a carbon–sulfur silica–calcite

diffraction peak at 23.5° . Thus, combined sulfate freeze–thaw action causes carbon–sulfur silica–calcite erosion in concrete.

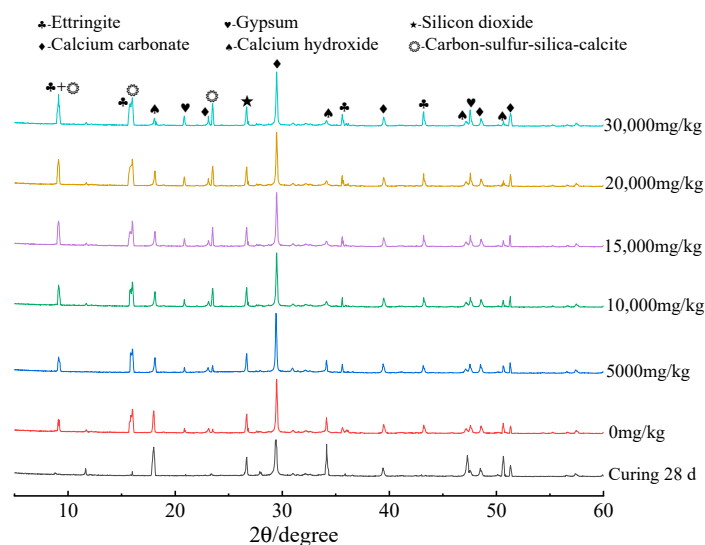


Figure 5. XRD plots of the sulfate freeze–thaw coupling 225 times.

3.3. Infrared Spectral Analysis

3.3.1. Full Immersion Test of Concrete

According to currently available research [34,35], $[\text{AlO}_6]$ occurs at approximately 850 cm^{-1} , the S–O stretch occurs at approximately 1100 cm^{-1} , and the O–H stretch occurs at approximately $3600\text{--}3200\text{ cm}^{-1}$. The bands that occur at 1420 , 874 , and 710 cm^{-1} and are attributed to the asymmetric ν_3 and symmetric ν_2 and ν_4 of C–O allow one to identify the CO_3^{2-} . The appearance of the C–O bands at 1465 and 874 cm^{-1} confirms the carbonation of the ettringite [36]. Figure 6 displays the results of infrared spectrogram tests conducted to further identify the kind of erosion products after the concrete specimens were submerged for 270 days at various sulfate concentrations. The appearance of C–O vibrational stretching peaks at 423 cm^{-1} and 715 cm^{-1} can be observed, suggesting the existence of CO_3^{2-} group-containing compounds in the specimens. This is a result of calcium carbonate being the primary component of aggregate. The existence of several SO_4^{2-} -containing groups in the specimen was indicated by the appearance of an S–O vibrational stretching peak at 1134 cm^{-1} . An Al–O vibrational stretching peak at 848 cm^{-1} suggests that the sample contains $[\text{AlO}_6]$ groups. The above illustrates the generation of calcite and gypsum inside the concrete specimens following their 270-day immersion in a sulfate environment. Moreover, the vibrational telescoping peaks of the individual chemical bonds gradually increased as the sulfate concentration increased, indicating an increase in the content of the individual substances.

Stretching vibration bands produced by the OH groups in portlandite at 3642 cm^{-1} and stretching and bending vibration bands ascribed to water at 3435 and 1634 cm^{-1} are reported in the literature that is currently available [37–39]. Therefore, the typical vibrational peak of the water molecule is located at about 3450 cm^{-1} . Concrete, on the other hand, is a mixture of minerals such as calcium hydroxide, gypsum, ettringite, and calcium silicate hydrate that include water molecules but do not mix with them in the same way, causing their vibration peaks to fluctuate in location.

3.3.2. Concrete Sulfate Freeze–Thaw Coupling Tests

The infrared spectra of the concrete sulfate freeze–thaw coupling test conditions are displayed in Figure 7. The C–O expansion ion vibration peaks that can be noticed at 1426 cm^{-1} and 717 cm^{-1} show that calcium carbonate is present inside the concrete specimens. The peak of the S–O stretching vibration, which showed the existence of gypsum inside the

specimen, is observed at 1113 cm^{-1} . Furthermore, the occurrence of the Al-O stretching vibration peak at 849 cm^{-1} indicates the presence of calcite in the erosion product. In contrast to the sulfate full immersion test following sulfate freeze–thaw coupling, the specimen has a distinctive SiO_6 vibrational peak at 501 cm^{-1} . Moreover, at sulfate immersion concentrations of $20,000\text{ mg/kg}$ and $30,000\text{ mg/kg}$, the distinctive vibrational peaks of SiO_6 are also visible in 752 cm^{-1} . Generally speaking, Si in materials containing Si is paired with other atoms or groups in a tetra-coordinated form; currently, the only material containing six-coordinated Si in a cement-based material system is carbon–sulfur silica–calcite [40]. Hence, under sulfate freeze–thaw coupling conditions, carbon–sulfur silica–calcite formation occurs, which is in line with the XRD findings.

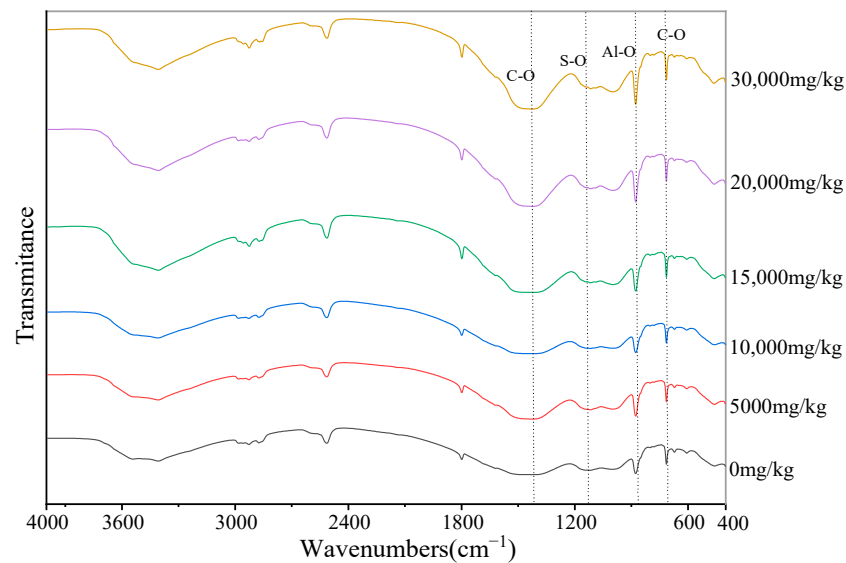


Figure 6. Infrared spectra of specimens immersed for 270 d at different sulfate concentrations.

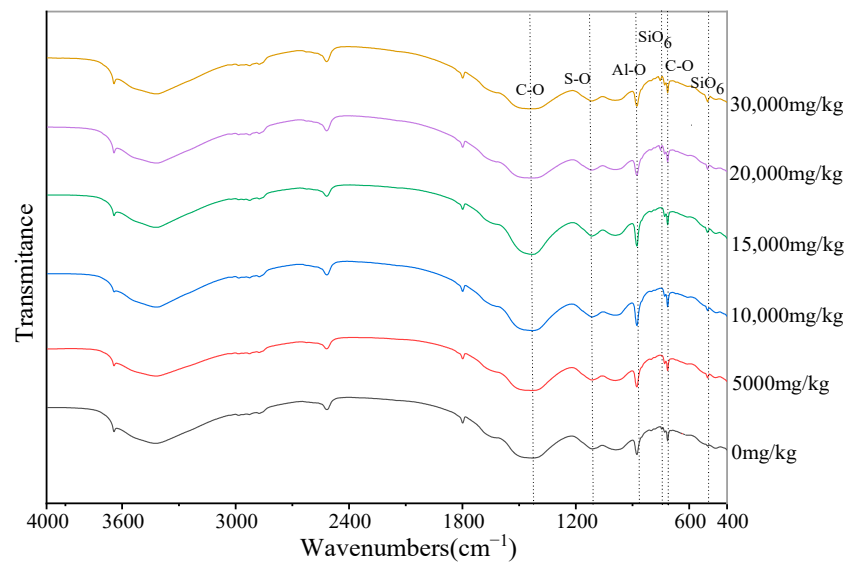


Figure 7. 225 freeze–thaw cycles infrared spectra at various sulfate concentrations.

3.4. SEM & EDS Analysis

3.4.1. Full Immersion Test of Concrete

Figures 8 and 9 (The energy spectrum plot on the right is obtained from the black dots in the red box.) display the SEM and EDS of the immersed concrete. The erosion products are primarily found in the interfacial zone and pores/cracks of the concrete specimens. This is mostly because the matrix of concrete is comparatively more porous than that of mortar,

which facilitates the passage of calcium ions, phases containing aluminum, and sulfate ions. The buildup of erosion products causes the internal concrete specimen expansion strains, microcracks, and bonding of the internal concrete material to decrease. As a result, cracks appear, the concrete specimen's macroscopically mechanical strength declines, and its microstructural strength is compromised. As can be seen from Figures 8 and 9, when the SO_4^{2-} concentration is 0 mg/kg, the concrete specimens are well hydrated after 28 days of curing, and the internal micro-morphology is structurally dense, but there are also initial micro-cracks existing. The concrete specimens have a significant amount of intact $\text{Ca}(\text{OH})_2$ crystals, as well as a substantial number of flocculent hydration products (C-S-H) filling the pores and microcracks within them, according to SEM imaging.

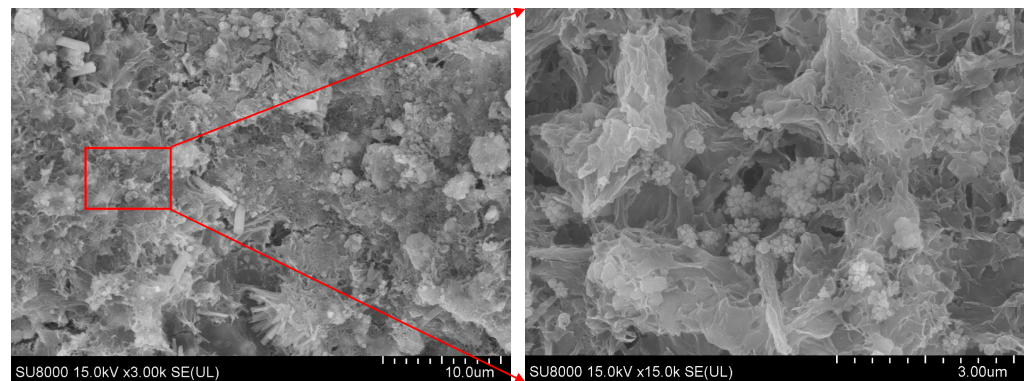


Figure 8. 0 mg/kg C-S-H gel in the pores of the specimen after 28 days of curing.

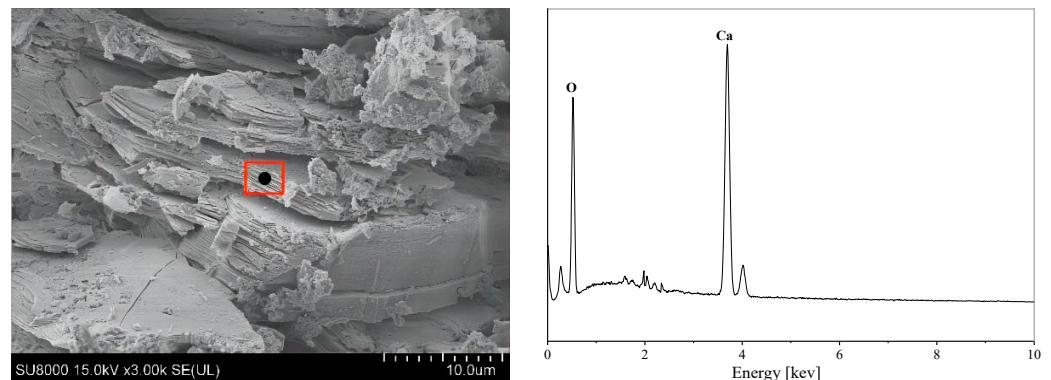


Figure 9. The $\text{Ca}(\text{OH})_2$ crystal in the specimen after 28 days of curing at 40 mg/kg.

The EDS energy spectra and microscopic morphology of concrete specimens submerged in various sulfate concentration solutions for 270 days are displayed in Figures 10–15. It can be observed that the acicular ettringite in the concrete pores is fibrously connected at low sulfate concentrations. Ettringite crystals gather in huge quantities in the pores and fissures at the boundary when the sulfate concentration rises, mostly as clusters or needle-like multiple interwoven roots. This ettringite in clusters has an excellent crystalline shape, grows from the pore's edge to its interior, absorbs water easily, enlarges, and frequently forms clusters perpendicular to the fissure's surface. This results in high internal tensions, which weaken the aggregate's attachment to the concrete specimen's paste and deteriorate qualities of the concrete. In the later stages of erosion, swelling materials continue to form, and the stresses induced by ettringite and gypsum are transferred to the cement matrix, leading to interfacial cracking [41]. Simultaneously, as the specimens gradually develop more fractures, more SO_4^{2-} ions diffuse into the interior of the concrete, and more erosion products are formed.

Additionally, it is evident from Figures 10–12 that ettringite erosion products in the form of needles occur in the pores of the concrete specimens, primarily exhibiting ettringite-type erosion when the sulfate content falls below 15,000 mg/kg. In addition, the amount of

ettringite increases with the concentration of exogenous sulfate. As the sulfate concentration increases, the amount of ettringite somewhat reduces, the lamellar erosion products grow, and the sulfate content rises inside the concrete specimen. The erosion products inside the concrete specimens were primarily gypsum and ettringite, indicating gypsum–ettringite-type erosion, at sulfate concentrations of 15,000–20,000 mg/kg. A significant amount of lamellar and short columnar gypsum is created inside the specimen at sulfate ion concentrations of 20,000–30,000 mg/kg because of the high sulfate circumstances that cause the concrete specimen to produce a significant amount of gypsum. Large amounts of gypsum are produced by the concrete sample, as seen in Figures 14 and 15, and the EDS spectra of the short and medium columnar erosion products reveal that Ca, S, and O make up the majority of their composition. This suggests that the short columnar crystals are composed primarily of gypsum and exhibit gypsum-type erosion.

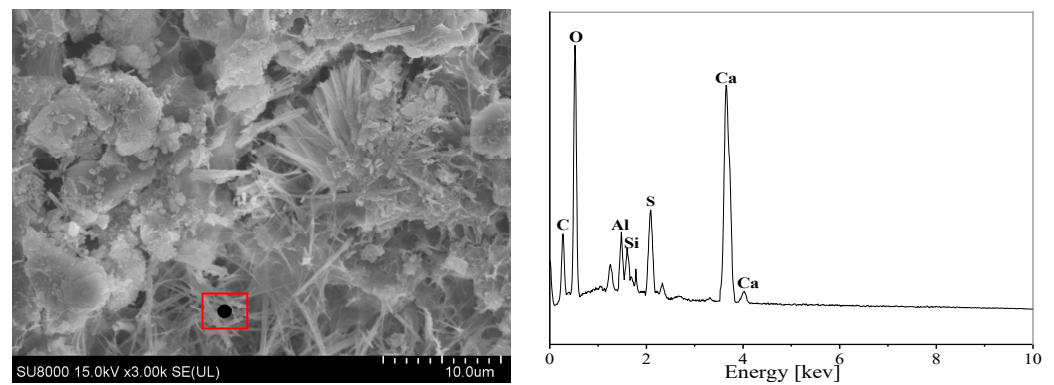


Figure 10. Micro-products of 270 days soaking at a concentration of 0 mg/kg.

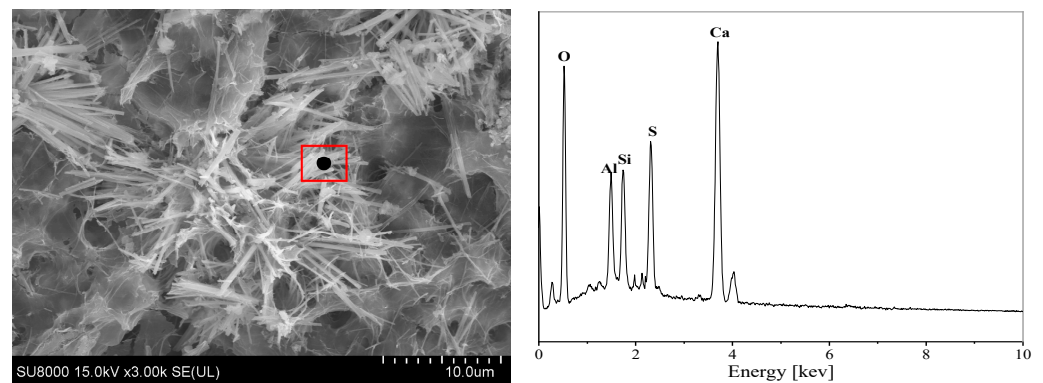


Figure 11. Micro-products of 270 days soaking at a concentration of 5000 mg/kg.

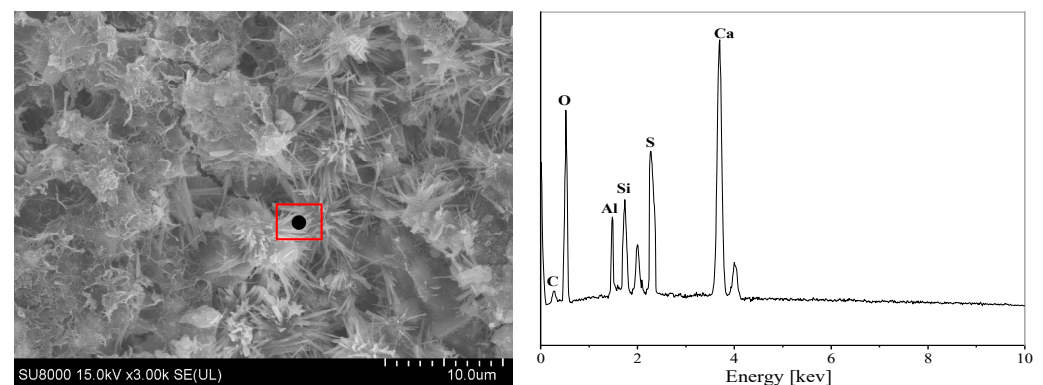


Figure 12. Micro-products of 270 days soaking at a concentration of 10,000 mg/kg.

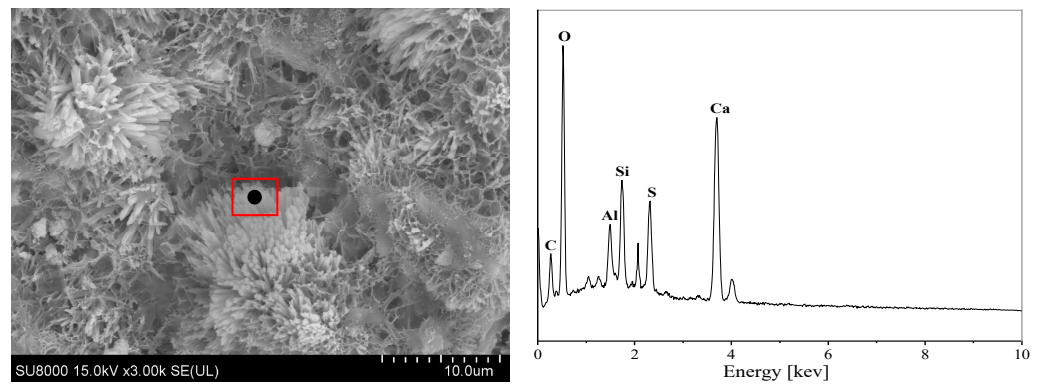


Figure 13. Micro-products of 270 days soaking at a concentration of 15,000 mg/kg.

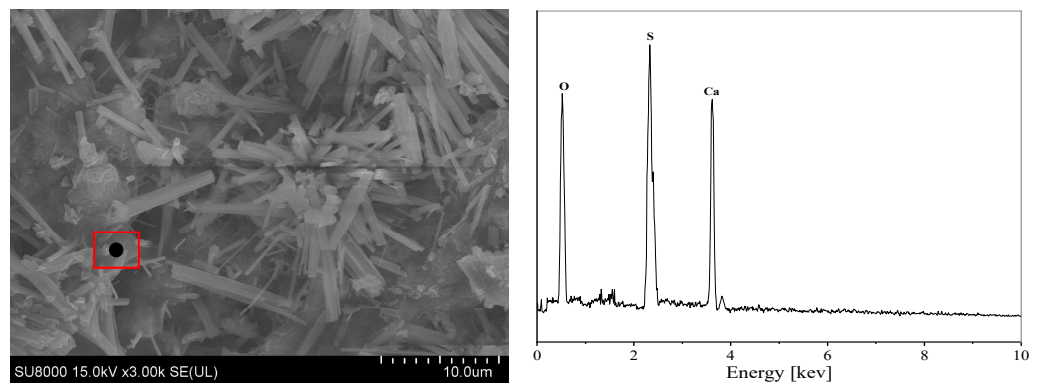


Figure 14. Micro-products of 270 days soaking at a concentration of 20,000 mg/kg.

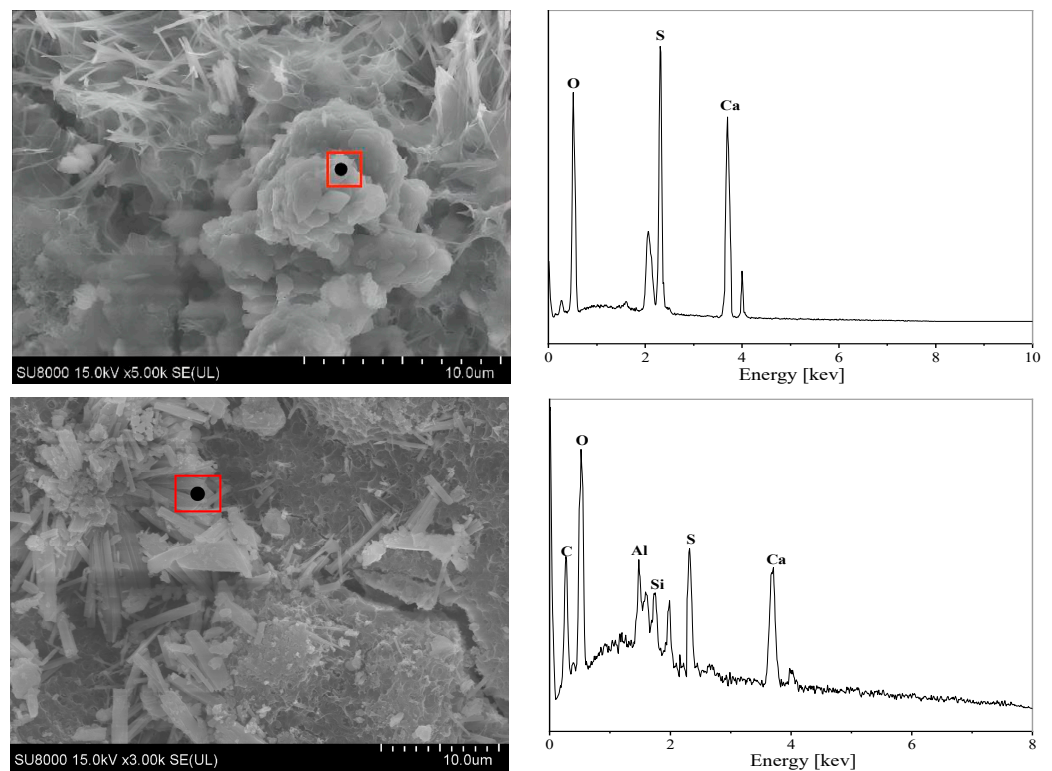


Figure 15. Micro-products of 270 days soaking at a concentration of 30,000 mg/kg.

As illustrated in Figure 16, many petal-like crystals are also discovered in micro-morphological studies at a concentration of 30,000 mg/kg on the concrete specimen's

edge. Based on energy spectrum research, the composition of these petal-like crystals is primarily Na, S, and O, suggesting that they are crystals of sodium sulfate. This suggests that, particularly at high concentrations of sulfate solution, the process of sulfate assault is also followed by the crystallization of sodium sulfate, as seen by the white coating of crystalline salt that covers the outside of the concrete test samples.

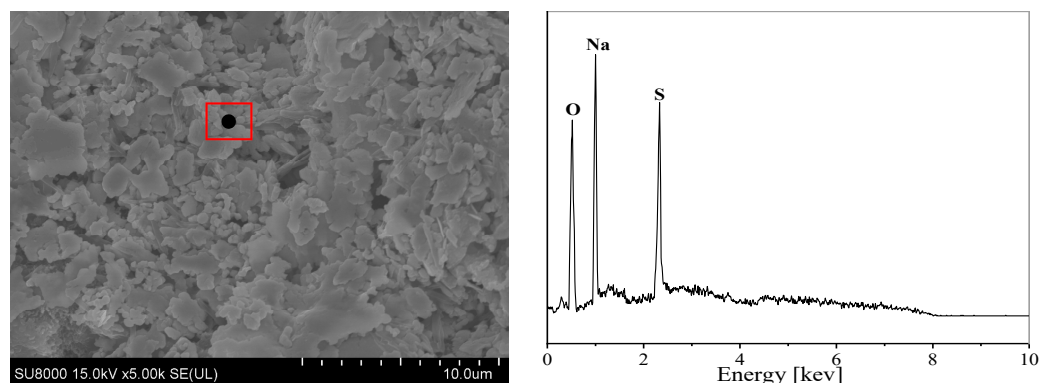


Figure 16. Microscopic analysis of boundary crystal of 30,000 mg/kg concrete specimen.

The erosion products within the concrete specimens are primarily ettringite at low sulfate concentrations (<15,000 mg/kg), according to a combination of XRD, infrared spectroscopy, and scanning electron microscopy (SEM). Inside the concrete specimen, gypsum starts to form as the sulfate content progressively rises. The primary erosion products found within the specimen are gypsum and ettringite. Short columnar and lamellar gypsum products are visible inside the concrete specimens once the concentration reaches 20,000 mg/kg, and the XRD gypsum diffraction peak intensity is noticeably increased.

3.4.2. Concrete Sulfate Freeze–Thaw Coupling Tests

Concrete damage from freeze–thaw cycles primarily takes the form of surface spalling and interior disintegration [42]. Freeze–thaw cycles in the concrete specimen cause the water within its pores to expand and freeze, creating microcracks in the internal structure that allow SO_4^{2-} from the environment to enter the interior of the concrete [43,44]. Thus, when concrete specimens are exposed to sulfate freeze–thaw coupling, the deterioration of the specimens is also more noticeable.

Upon 225 cycles of freezing and thawing at six different sulfate concentrations, the concrete specimens exhibited noticeable fractures, as depicted in Figure 17, and many needle-shaped, short columnar crystals surfaced at the crack’s periphery. The SEM reveals that the products were calcite and gypsum. The appearance of these fissures in the concrete specimens made it easier for environmental SO_4^{2-} to infiltrate the inside of the specimens. SO_4^{2-} infiltrated the concrete specimens’ pores by differential pressure infiltration. This resulted in a rise in the concentration of SO_4^{2-} in the concrete specimens’ pores, as well as an increase in the number of ettringite crystals and the formation of gypsum crystals. The large-scale growth of its products occurred mostly in the pores and boundaries of concrete, where they coexisted with fractures. Microcracks in the concrete specimen occurred when the expansion stress of the erosion products surpassed the tensile strength of the specimen. The specimen’s internal cracks enlarged and widened as the coupling action went on, damaging the concrete specimen’s structure and drastically lowering its strength.

Low temperature creates a generative setting for paired sulfate freeze–thaw conditions of carbon–sulfur calcium silica [45]. The XRD and infrared physical phase analysis unequivocally demonstrates that the freeze–thaw environment inside the concrete specimens produced carbon–sulfur silica–calcite. Yet, chalcocite, which likewise has acicular and clustered crystal structures, and carbon–sulfur silica–calcite share a very similar crystal structure. All that is different, though, is that the carbon–sulfur silica–calcite crystals are shorter than the ettringite crystals. The concrete had a significant number of needle-like,

clustered crystals, all of which were less than 5 μm , as seen in Figure 18. By using EDS energy spectral spot scanning, the primary compositions of Ca, Si, Al, S, O, and C show that these small crystals are carbon–sulfur silica–calcite crystals.

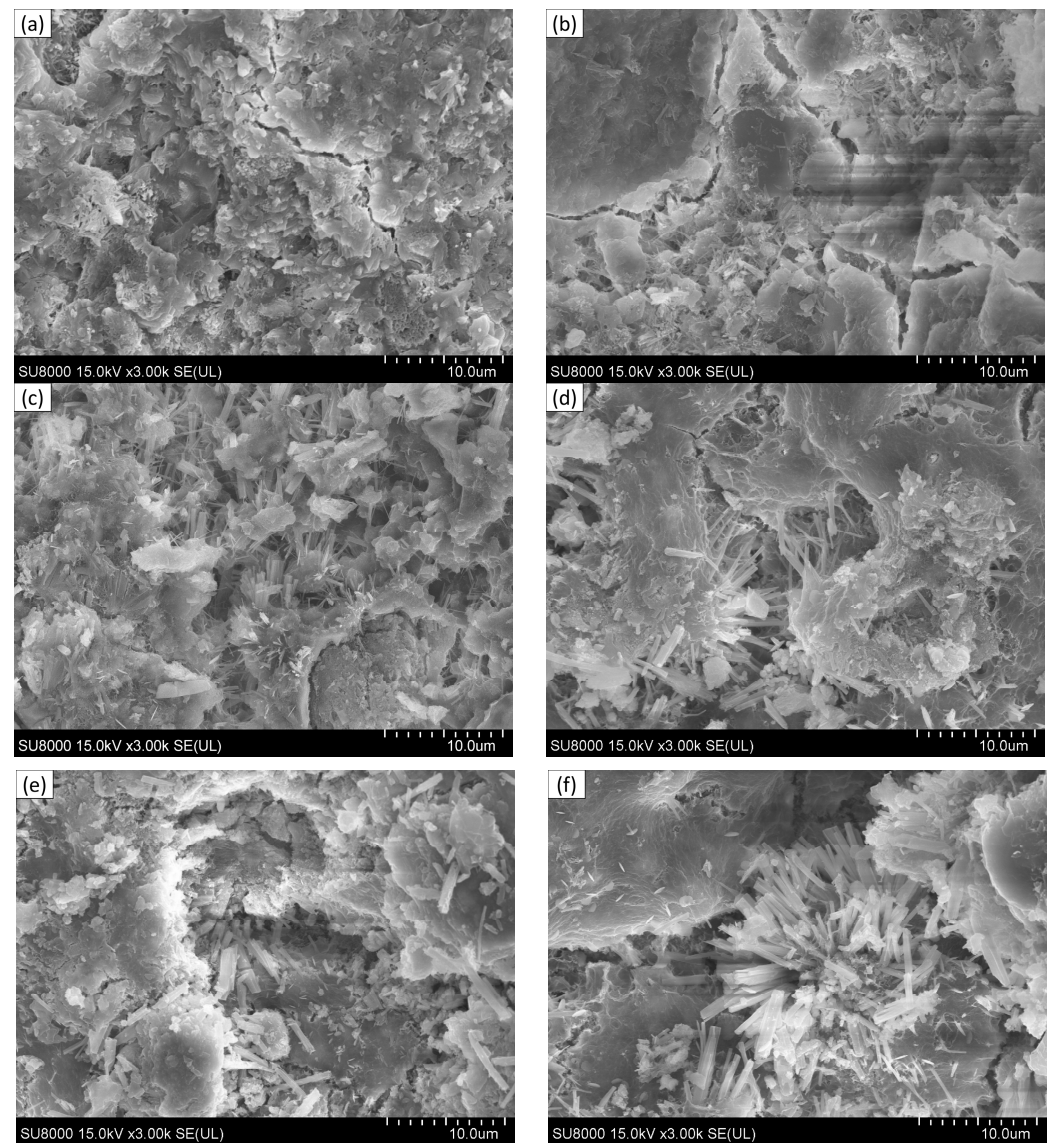


Figure 17. SEM images of concrete specimens after 225 freeze–thaw cycles. (a) 0 mg/kg; (b) 5000 mg/kg; (c) 10,000 mg/kg; (d) 15,000 mg/kg; (e) 20,000 mg/kg; (f) 30,000 mg/kg.

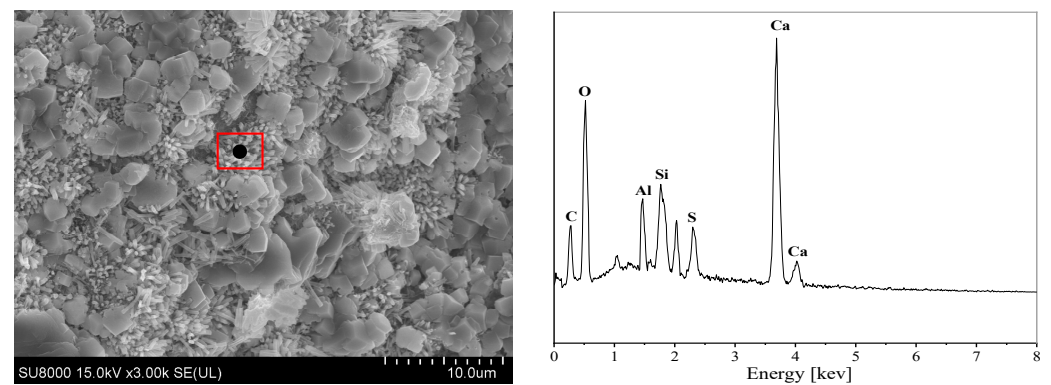


Figure 18. SEM images of concrete specimens after 225 freeze–thaw cycles at 30,000 mg/kg.

3.5. Classification of Concrete Sulfate Erosion Damage Types in Tumushuke Area

The sulfate freeze–thaw coupling test and the total immersion test were conducted using six sets of sulfate solutions varying in concentration: 0 mg/kg, 5000 mg/kg, 10,000 mg/kg, 15,000 mg/kg, 20,000 mg/kg, and 30,000 mg/kg. It was discovered that when the sulfate content was less than 15,000 mg/kg, the concrete specimens primarily exhibited ettringite-type erosion. Under the full immersion test circumstances, ettringite predominated in the erosion products. At 15,000–20,000 mg/kg, the specimens had an ettringite–gypsum type of erosion, and at 20,000–30,000 mg/kg, gypsum predominated in the erosion products, and the specimens displayed a gypsum-type of erosion. A small amount of ettringite and gypsum, as well as carbon–sulfur calcium silica, was produced by the concrete specimens' reaction with the carbonate within the concrete during the sulfate freeze–thaw coupling test conditions. The specimens also primarily displayed carbon–sulfur silica–calcite-type erosion. To categorize the several types of sulfate erosion damage that concrete buildings in the Tumushuke area would be largely subjected to, the test results were thoroughly examined. According to the sulfate concentration distribution map for the Tumushuke area, the soil has a high concentration of SO_4^{2-} , which is very caustic to the concrete buildings in the region. Most of the locations have sulfate concentrations of less than 15,000 mg/kg [6], meaning that calcareous erosion is the primary kind of erosion damage to concrete. These regions are mostly located in the Tumushuke area's southwest and northeastern sections, with the central–northern region, which is distinguished by ettringite–gypsum- and gypsum-type erosion, possessing higher sulfate concentrations. The distribution of its types is shown in Figure 19.

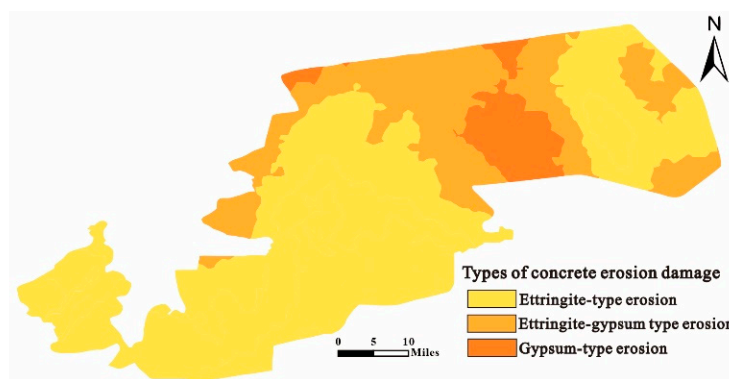


Figure 19. Division of concrete erosion damage types in the Tumushuke area.

4. Conclusions and Perspectives

The study area was the Tumushuke area in southern Xinjiang, and the full sulfate immersion and sulfate freeze–thaw coupling test procedures were applied. The microstructure of concrete was investigated using SEM, XRD, infrared analysis, and other microanalytical instruments, and the physical phase composition of erosion products in various erosion conditions was ascertained to categorize the type of erosion damage. The findings of the study may have significant engineering applications in lowering project costs and using various anti-sulfate erosion strategies during the development of future projects.

- (1) Concrete displays three different types of erosion: ettringite-type erosion occurs when the sulfate concentration is less than 15,000 mg/kg, ettringite–gypsum erosion occurs between 15,000 and 20,000 mg/kg, and gypsum erosion predominates when the concentration exceeds 20,000 mg/kg. Carbon–sulfur silica–calcite erosion will also occur in concrete under sulfate freeze–thaw coupling.
- (2) The Tumushuke area's southern and northeastern regions have low sulfate concentrations and primarily exhibit ettringite–gypsum-type erosion damage. In contrast, the center north has high sulfate concentrations and primarily exhibits gypsum-type and ettringite–gypsum-type erosion damage.

The paper only investigated the type of concrete erosion at a maximum sulfate concentration of 30,000 mg/kg, and only six gradients of the erosion solution were selected. Subsequently, more concentration gradients could be set, potentially leading to a more comprehensive delineation of erosion types in different areas throughout the Tumushuke area. In the future, different anti-erosion measures can be adopted for different areas according to the division of concrete sulfate erosion types in the Tumushuke area to reduce the cost of project construction. At the same time, it lays the foundation for the subsequent adoption of different anti-erosion measures in different engineering and construction areas.

Author Contributions: Y.M.: conceptualization, methodology, data curation, and writing—original draft; X.J.: writing—review and formal analysis; J.L. and G.L.: supervision, writing—review, project administration and funding acquisition; W.H. and W.C.: resources and formal analysis; G.C. and Z.Y.: validation and writing—review. All authors have read and agreed to the published version of the manuscript.

Funding: This research was supported and funded by the Natural Science Foundation of China (52168064), the Science and Technology Project of Bingtuan (2021DB005), and Sichuan regional innovation cooperation project (2021YFQ0021).

Data Availability Statement: The original contributions presented in this study are included in the article. Further inquiries may be directed to the appropriate author.

Conflicts of Interest: Authors Wei Huang and Guangming Cao were employed by the company Xinjiang Qiankun Engineering Construction Group. The remaining authors declare that the research was conducted in the absence of any commercial or financial relationships that could be construed as a potential conflict of interest.

References

1. Yang, D.; Yan, C.; Zhang, J.; Liu, S.; Li, J. Chloride threshold value and initial corrosion time of steel bars in concrete exposed to saline soil environments. *Constr. Build. Mater.* **2021**, *267*, 120979. [[CrossRef](#)]
2. Zhao, G.; Li, J.; Shi, M.; Cui, J.; Xie, F. Degradation of cast-in-situ concrete subjected to sulphate-chloride combined attack. *Constr. Build. Mater.* **2020**, *241*, 117995. [[CrossRef](#)]
3. Liao, K.-X.; Zhang, Y.-P.; Zhang, W.-P.; Wang, Y.; Zhang, R.L. Modeling constitutive relationship of sulfate-attacked concrete. *Constr. Build. Mater.* **2020**, *260*, 119902. [[CrossRef](#)]
4. Yu, D.; Feng, C.; Fu, T.; Shen, A. Effect of Sulfate Concentration on Chloride Diffusion of Concrete under Cyclic Load. *Materials* **2022**, *15*, 2036. [[CrossRef](#)] [[PubMed](#)]
5. Wang, K.; Guo, J.J.; Yang, L.; Zhang, P.; Xu, H.Y. Multiphysical damage characteristics of concrete exposed to external sulfate attack: Elucidating effect of drying-wetting cycles. *Constr. Build. Mater.* **2022**, *329*, 127143. [[CrossRef](#)]
6. Jiang, X.; Ma, Y.; Li, G.; Huang, W.; Zhao, H.; Cao, G.; Wang, A. Spatial Distribution Characteristics of Soil Salt Ions in Tumushuke City, Xinjiang. *Sustainability* **2022**, *14*, 16486. [[CrossRef](#)]
7. Klein, N.; Gómez, E.D.; Duffó, G.S.; Farina, S.B. Effect of sulphate on the corrosion of reinforcing steel in concrete. *Constr. Build. Mater.* **2022**, *354*, 129214. [[CrossRef](#)]
8. Liu, Z.; Zhang, F.; Deng, D.; Xie, Y.; Long, G.; Tang, X. Physical sulfate attack on concrete lining—A field case analysis. *Case Stud. Constr. Mater.* **2017**, *6*, 206–212. [[CrossRef](#)]
9. Wu, J.; Wei, J.; Huang, H.; Hu, J.; Yu, Q. Effect of multiple ions on the degradation in concrete subjected to sulfate attack. *Constr. Build. Mater.* **2020**, *259*, 119846. [[CrossRef](#)]
10. Idiart, A.E.; López, C.M.; Carol, I. Chemo-mechanical analysis of concrete cracking and degradation due to external sulfate attack: A meso-scale model. *Cem. Concr. Compos.* **2011**, *33*, 411–423. [[CrossRef](#)]
11. Cheng, H.; Liu, T.; Zou, D.; Zhou, A. Compressive strength assessment of sulfate-attacked concrete by using sulfate ions distributions. *Constr. Build. Mater.* **2021**, *293*, 123550. [[CrossRef](#)]
12. Ragoug, R.; Metalssi, O.O.; Barberon, F.; Torrenti, J.-M.; Roussel, N.; Divet, L.; d’Espinose de Lacaillerie, J.-B. Durability of cement pastes exposed to external sulfate attack and leaching: Physical and chemical aspects. *Cem. Concr. Res.* **2019**, *116*, 134–145. [[CrossRef](#)]
13. Shen, X.M.; Yang, H.Q.; Li, X.; Li, M.X. Progress and Review of Research on Durability of Hydraulic Concrete under Alternate Freeze-Thaw and Carbonation Effected by Wet-Dry Cycles. *Appl. Mech. Mater.* **2013**, *405–408*, 2734–2738. [[CrossRef](#)]
14. Zhao, N.; Wang, S.; Wang, C.; Quan, X.; Yan, Q.; Li, B. Study on the durability of engineered cementitious composites (ECCs) containing high-volume fly ash and bentonite against the combined attack of sulfate and freezing-thawing (F-T). *Constr. Build. Mater.* **2020**, *233*, 123550. [[CrossRef](#)]

15. Sotiriadis, K.; Mácová, P.; Mazur, A.S.; Viani, A.; Tolstoy, P.M.; Tsivilis, S. Long-term thaumasite sulfate attack on Portland-limestone cement concrete: A multi-technique analytical approach for assessing phase assemblage. *Cem. Concr. Res.* **2020**, *130*, 105995. [[CrossRef](#)]
16. Zhao, G.; Li, J.; Shi, M.; Fan, H.; Cui, J.; Xie, F. Degradation mechanisms of cast-in-situ concrete subjected to internal-external combined sulfate attack. *Constr. Build. Mater.* **2020**, *248*, 118683. [[CrossRef](#)]
17. He, W.; Li, B.; Meng, X.; Shen, Q. Compound Effects of Sodium Chloride and Gypsum on the Compressive Strength and Sulfate Resistance of Slag-Based Geopolymer Concrete. *Buildings* **2023**, *13*, 675. [[CrossRef](#)]
18. GB/T 50082-2009; Standard for Test Methods of Long-Term Performance and Durability of Ordinary Concrete. Standards Press of China: Beijing, China, 2009.
19. GB/T 50081-2019; Standard for Test Method of Mechanical and Physical Performance on Concrete. Standards Press of China: Beijing, China, 2019.
20. Liu, J.; Zang, S.; Yang, F.; Zhang, M.; Li, A. Fracture Mechanical Properties of Steel Fiber Reinforced Self-Compacting Concrete under Dry–Wet Cycle Sulfate Attack. *Buildings* **2022**, *12*, 1623. [[CrossRef](#)]
21. Zhou, S.; Ju, J.W. A chemo-micromechanical damage model of concrete under sulfate attack. *Int. J. Damage Mech.* **2021**, *30*, 1213–1237. [[CrossRef](#)]
22. Müllauer, W.; Beddoe, R.E.; Heinz, D. Sulfate attack expansion mechanisms. *Cem. Concr. Res.* **2013**, *52*, 208–215. [[CrossRef](#)]
23. Shen, X.Y.; Feng, P.; Zhang, Q.; Lu, J.Y.; Liu, X.; Ma, Y.F.; Jin, P.; Wang, W.; Ran, Q.P.; Hong, J.X. Toward the formation mechanism of synthetic calcium silicate hydrate (C-S-H)-pH and kinetic considerations. *Cem. Concr. Res.* **2023**, *172*, 107248. [[CrossRef](#)]
24. Liu, X.; Feng, P.; Li, W.; Geng, G.Q.; Huang, J.L.; Gao, Y.; Mu, S.; Hong, J.X. Effects of pH on the nano/micro structure of calcium silicate hydrate (C-S-H) under sulfate attack. *Cem. Concr. Res.* **2021**, *140*, 106306. [[CrossRef](#)]
25. Tao, Y.; Gao, Y.N.; Sun, Y.J.; Pellenq, R.J.M.; Poon, C.S. C-S-H decalcification in seawater: The view from the nanoscale. *Cem. Concr. Res.* **2024**, *175*, 107385. [[CrossRef](#)]
26. Chen, J.J.; Thomas, J.J.; Taylor, H.F.W.; Jennings, H.M. Solubility and structure of calcium silicate hydrate. *Cem. Concr. Res.* **2004**, *34*, 1499–1519. [[CrossRef](#)]
27. Ma, X.; Çopuroglu, O.; Schlangen, E.; Han, N.X.; Xing, F. Expansion and degradation of cement paste in sodium sulfate solutions. *Constr. Build. Mater.* **2018**, *158*, 410–422. [[CrossRef](#)]
28. Liu, F.; Zhang, T.H.; Luo, T.; Zhou, M.Z.; Zhang, K.K.; Ma, W.W. Study on the Deterioration of Concrete under Dry-Wet Cycle and Sulfate Attack. *Materials* **2020**, *13*, 4095. [[CrossRef](#)] [[PubMed](#)]
29. Liu, Z.; Li, X.; Deng, D.; De Schutter, G.; Hou, L. The role of Ca(OH)₂ in sulfate salt weathering of ordinary concrete. *Constr. Build. Mater.* **2016**, *123*, 127–134. [[CrossRef](#)]
30. Wang, C.; Xiao, J.; Long, C.; Zhang, Q.; Shi, J.; Zhang, Z. Influences of the joint action of sulfate erosion and cementitious capillary crystalline waterproofing materials on the hydration products and properties of cement-based materials: A review. *J. Build. Eng.* **2023**, *68*, 106061. [[CrossRef](#)]
31. Yuan, X.; Dai, M.; Li, M.; Liu, F. Study of the Freeze–Thaw Resistance for Composite Fiber Recycled Concrete with Sulphate Attack Exposure. *Buildings* **2023**, *13*, 1037. [[CrossRef](#)]
32. Cefis, N.; Tedeschi, C.; Comi, C. External sulfate attack in structural concrete made with Portland-limestone cement: An experimental study. *Can. J. Civ. Eng.* **2021**, *48*, 731–739. [[CrossRef](#)]
33. Zhou, Y.; Ma, B.; Huang, J.; Li, X.; Tan, H.; Lv, Z. Influence of Ca/Si ratio of concrete pore solution on thaumasite formation. *Constr. Build. Mater.* **2017**, *153*, 261–267. [[CrossRef](#)]
34. Abubaker, F.; Lynsdale, C.; Cripps, J. Investigation of concrete-clay interaction with regards to the thaumasite form of sulfate attack. *Constr. Build. Mater.* **2014**, *67*, 88–94. [[CrossRef](#)]
35. Barnett, S.J.; Macphee, D.E.; Lachowski, E.E.; Crammond, N.J. XRD, EDX and IR analysis of solid solutions between thaumasite and ettringite. *Cem. Concr. Res.* **2002**, *32*, 719–730. [[CrossRef](#)]
36. Ghorab, H.Y.; Mabrouk, M.R.; Herfort, D.; Osman, Y.A. Infrared investigation on systems related to the thaumasite formation at room temperature and 7 °C. *Cem. Wapno Beton* **2014**, *19*, 252.
37. Scholtzová, E.; Kucková, L.; Kozísek, J.; Pálková, H.; Tunega, D. Experimental and computational study of thaumasite structure. *Cem. Concr. Res.* **2014**, *59*, 66–72. [[CrossRef](#)]
38. Carmona-Quiroga, P.M.; Blanco-Varela, M.T. Use of barium carbonate to inhibit sulfate attack in cements. *Cem. Concr. Res.* **2015**, *69*, 96–104. [[CrossRef](#)]
39. Myneni SC, B.; Traina, S.J.; Waychunas, G.A.; Logan, T.J. Vibrational spectroscopy of functional group chemistry and arsenate coordination in ettringite. *Geochim. Et Cosmochim. Acta* **1998**, *62*, 3499–3514. [[CrossRef](#)]
40. Mittermayr, F.; Baldermann, A.; Kurta, C.; Rinder, T.; Klammer, D.; Leis, A.; Tritthart, J.; Dietzel, M. Evaporation—A key mechanism for the thaumasite form of sulfate attack. *Cem. Concr. Res.* **2013**, *49*, 55–64. [[CrossRef](#)]
41. He, R.; Zheng, S.N.; Gan, V.J.L.; Wang, Z.D.; Fang, J.H.; Shao, Y. Damage mechanism and interfacial transition zone characteristics of concrete under sulfate erosion and Dry-Wet cycles. *Constr. Build. Mater.* **2020**, *255*, 119340. [[CrossRef](#)]
42. Luan, H.; Wu, J.; Pan, J. Freeze-thaw Durability of Recycled Aggregate Concrete: An Overview. *J. Wuhan Univ. Technol.-Mater. Sci. Ed.* **2021**, *36*, 58–69. [[CrossRef](#)]
43. Wang, J.; Zhang, J.; Cao, D. Pore characteristics of recycled aggregate concrete and its relationship with durability under complex environmental factors. *Constr. Build. Mater.* **2021**, *272*, 121642. [[CrossRef](#)]

44. Zhang, M.; Lv, H.; Zhou, S.; Wu, Y.; Zheng, X.; Yan, Q. Study on the Frost Resistance of Composite Limestone Powder Concrete against Coupling Effects of Sulfate Freeze–Thaw. *Buildings* **2023**, *13*, 2776. [[CrossRef](#)]
45. Schovanz, D.; Tiecher, F.; Hasparyk, N.P.; Kuperman, S.; Lermen, R.T. Evaluation of Delayed Ettringite Formation through Physical, Mechanical, and Microstructural Assays. *ACI Mater. J.* **2021**, *118*, 101–109.

Disclaimer/Publisher’s Note: The statements, opinions and data contained in all publications are solely those of the individual author(s) and contributor(s) and not of MDPI and/or the editor(s). MDPI and/or the editor(s) disclaim responsibility for any injury to people or property resulting from any ideas, methods, instructions or products referred to in the content.